Title

Kinase fusions are frequent in Spitz tumours and spitzoid melanomas

Journal

Nature Communications, 5(1)

ISSN

2041-1723

Authors

Wiesner, Thomas

He, Jie

Yelensky, Roman

et al.

Publication Date

2014

DOI

10.1038/ncomms4116

Peer reviewed

Published in final edited form as:
Nat Commun. 2014 ; 5: 3116. doi:10.1038/ncomms4116.

Kinase fusions are frequent in Spitz tumors and spitzoid melanomas

Thomas Wiesner[#1,2], **Jie He**[#3], **Roman Yelensky**[#3], **Rosaura Esteve-Puig**[4], **Thomas Botton**[4], **Iwei Yeh**[4], **Doron Lipson**[3], **Geoff Otto**[3], **Kristina Brennan**[3], **Rajmohan Murali**[1,6], **Maria Garrido**[4], **Vincent A. Miller**[3], **Jeffrey S Ross**[3], **Michael F. Berger**[1], **Alyssa Sparatta**[4], **Gabriele Palmedo**[5], **Lorenzo Cerroni**[2], **Klaus J. Busam**, **Heinz Kutzner**[5], **Maureen T Cronin**[3], **Philip J Stephens**[3], and **Boris C. Bastian**[1,4,6]

[1]Human Oncology and Pathogenesis Program, Memorial Sloan-Kettering Cancer Center, 415 E 68th Street, New York, New York 10065, USA

[2]Department of Dermatology and Venereology, Medical University of Graz, Auenbruggerplatz 8, 8036 Graz, Austria

[3]Foundation Medicine, 1 Kendall Sq B6501, Cambridge, Massachusetts 02139, USA

[4]Departments of Dermatology and Pathology, UCSF Cardiovascular Research Institute, 555 Mission Bay Blvd. South, Room 252K, Box 3118, San Francisco, California 94158-9001, USA

[5]Dermatopathologie Friedrichshafen, Siemensstraße 6/1, 88048 Friedrichshafen, Germany

[6]Department of Pathology, Memorial Sloan-Kettering Cancer Center, 1275 York Avenue New York, New York 10065, USA.

[#] These authors contributed equally to this work.

Abstract

Spitzoid neoplasms are a group of melanocytic tumors with distinctive histopathologic features. They include benign tumors (Spitz nevi), malignant tumors (spitzoid melanomas), and tumors with borderline histopathologic features and uncertain clinical outcome (atypical Spitz tumors). Their genetic underpinnings are poorly understood, and alterations in common melanoma-associated oncogenes are typically absent. Here we show that spitzoid neoplasms harbor kinase

Correspondence and requests for materials should be addressed to P.J.S. (pstephens@foundationmedicine.com) or B.C.B (boris.bastian@ucsf.edu)..

AUTHOR CONTRIBUTION

Project planning and experimental design: T.W., J.H, R.Y., M.F.B., M.C., P.J.S., B.C.B.; Sample collection: T.W., H.K., G.P., L.C., K.J.B., B.C.B.; Preparation of DNA and cDNA libraries: K.B; Sequence data analysis: T.W., J.H., R.Y., D.L.; Generation of the translocation constructs: R.E.P, T.B., I.Y; Expression vector generation: R.E.P, T.B., I.Y.; In-vitro experiments including viral transfections and western blotting: R.E.P, T.B., I.Y, A.S.; In vivo experiments: T.B.; Review of histology and immunohistochemistry: T.W., H.K., L.C., K.J.B., B.C.B.; FISH analysis: T.W., M.G., A.S; Manuscript writing: T.W., R.M., P.J.S., B.C.B.; Review of the final manuscript: all authors.

COMPETING FINANCIAL INTERESTS

B.C.B., M.C., J.E., D.L., P.J.S., T.W., R.Y. are the authors of patent application under Application Serial No. US 61/768,340 (Novel fusion molecules and uses thereof). J.H., R.Y., J.S.R, D.L., K.B., V.M, P.J.S. are employees and stockholders of Foundation Medicine, Inc. The remaining authors declare no competing financial interests.

ACCESSION CODES

Sequence data have been deposited in NCBI/Genebank under the accession number YYYYY.

fusions of *ROS1* (17%), *NTRK1* (16%), *ALK* (10%), *BRAF* (5%), and *RET* (3%) in a mutually exclusive pattern. The chimeric proteins are constitutively active, stimulate oncogenic signaling pathways, are tumorigenic, and are found in the entire biologic spectrum of spitzoid neoplasms, including 55% of Spitz nevi, 56% of atypical Spitz tumors, and 39% of spitzoid melanomas. Kinase inhibitors suppress the oncogenic signaling of the fusion proteins *in vitro*. In summary, kinase fusions account for the majority of oncogenic aberrations in spitzoid neoplasms, and may serve as therapeutic targets for metastatic spitzoid melanomas.

Melanocytic neoplasms comprise several tumor types that are characterized by distinct clinical, pathologic, and genetic features. The clinical course of melanocytic tumors may be indolent (benign nevi), aggressive (malignant melanomas), or intermediate (melanocytic tumors of uncertain malignant potential).

In 1948, Sophie Spitz coined the term ‘melanoma of childhood’ for a group of melanocytic skin tumors composed of spindled or epithelioid melanocytes that developed predominantly in children and adolescents.[1] It later became clear that these tumors could also arise later in life, and that the majority of these neoplasms behaved in an indolent fashion, which led to the introduction of the term ‘Spitz nevus’ to indicate their benign nature. Malignant tumors with spitzoid histologic features were termed ‘spitzoid melanomas’, and these tumors often showed aggressive clinical behavior with widespread metastasis, similar to conventional melanomas. Tumors with histologic features overlapping those of Spitz nevi and spitzoid melanoma have been termed ‘atypical Spitz tumors’. Atypical Spitz tumors have the capacity to metastasize, but this is usually limited to the regional lymph nodes, and has little effect on patient survival.[2,3]

Genetic alterations in the majority of spitzoid neoplasms are not known, and they lack mutations in melanoma-associated oncogenes such as *NRAS, KIT, GNAQ* or *GNA11*.[4] However, subsets of spitzoid neoplasms characterized by distinct histopathologic features show *HRAS* mutations[5], or *BRAF* mutations combined with bi-allelic *BAP1* loss[6,7], suggesting that activation of kinase pathways plays an important role in the pathogenesis of these tumors. Identification of additional genetic events in kinase pathways may contribute to a better understanding of the pathogenesis of spitzoid neoplasms, and may facilitate the development of effective targeted therapies for metastasizing tumors, as illustrated by the success of small molecule kinase inhibitors in prolonging the lives of patients with a broad range of malignancies.[8-10]

For diagnostic reasons, spitzoid neoplasms are usually formalin-fixed and paraffin-embedded (FFPE) in their entirety, and nucleic acids isolated from FFPE tissue are typically degraded and of suboptimal quality. In addition, the percentage of neoplastic cells in spitzoid neoplasms is frequently low, due to the presence of varying numbers of admixed non-neoplastic lymphocytes, fibroblasts, and keratinocytes. The suboptimal quality of extracted nucleic acids and the low proportion of neoplastic melanocytic cells makes the identification of genetic aberrations in spitzoid neoplasms challenging and therefore a high sequencing coverage is necessary. For these reasons, we chose a massively parallel sequencing approach with high sequencing coverage for previously described cancer genes to investigate genetic aberrations in spitzoid neoplasms.

Our genomic analysis of 140 spitzoid neoplasms reveals gene rearrangements of the kinases *ROS1* (17%; n=24), *NTRK1* (16%; n=23), *ALK* (10%; n=14), *BRAF* (5%; n=7), and *RET* (3%; n=4) resulting in in-frame kinase fusions. These kinase fusions occur across the entire biologic spectrum of spitzoid neoplasms, including Spitz nevi (55%, fusions in 41 of 75 cases), atypical Spitz tumors (56%; fusions in 18 of 32 cases), and spitzoid melanomas (39%; fusions in 13 of 33 cases). The chimeric proteins appear in a mutually exclusive pattern, are constitutively active, stimulate oncogenic signaling pathways, are tumorigenic and may serve as diagnostic markers and as therapeutic targets for aggressive or metastasizing Spitz tumors.

RESULTS

Identification of Kinase Fusions

We investigated genomic alterations in a discovery cohort of 30 Spitz nevi and 8 atypical Spitz tumors by targeted massively parallel sequencing (Supplementary Table S1 summarizes the clinical, histopathologic and genetic data). For targeted DNA sequencing, we sequenced 3230 exons from 182 cancer-related genes and 37 introns of 14 genes commonly rearranged genes in cancer. We obtained an average unique coverage of 997x, with 99.96% of exons being sequenced at ≥100x coverage. In addition, we performed targeted transcriptome sequencing for 612 transcripts of kinases and kinase-related genes and achieved an average of 56,588,548 unique read pairs per spitzoid neoplasm. Six tumors (16%) harbored *HRAS* c.182A>T (p.Q61L) mutations and exhibited histopathologic features characteristic of the previously-described *HRAS*-mutant Spitz nevus variant.[5] Additionally, we found mutations in *PKHD1*, *ERBB4*, *LRP1B*, and amplifications of *MCL1* and *CCNE1* in one case each (Fig. 1a). No sequence alterations were found in the known melanoma oncogenes *BRAF*, *NRAS*, *KIT*, *GNAQ*, or *GNA11* or in other cancer-related genes listed in Supplementary Table 3.

Kinase fusions were identified in 18 of 30 (60%) Spitz nevi and in 6 of 8 (75%) atypical Spitz tumors (Fig. 1a and 1b). The rearrangements included gene fusions of the membrane-bound receptor tyrosine kinases *ROS1* (n=11, 29%), *ALK* (n=6, 16%), *NTRK1* (n=3, 8%), and *RET* (n=2, 5%). Two spitzoid neoplasms harbored t(7;19)(q34;q13) translocations that involved the serine/threonine kinase *BRAF*, but with different 5'-partners (*CEP89* and *LSM14A*) in each tumor. Using RT-PCR with breakpoint flanking primers, we verified that the fusion genes were expressed and produced in-frame transcripts. Using interphase FISH with breakpoint-flanking probes, we confirmed the disruptions at the *ROS1*, *ALK*, *NTRK1*, *RET*, and *BRAF* loci.

We validated our findings in an independent cohort of 102 spitzoid neoplasms using interphase FISH (Supplementary Table S2 summarizes the clinical, histopathologic and genetic data). In total, we analyzed 140 spitzoid neoplasms and identified fusions in 41 of 75 (55%) Spitz nevi, in 18 of 32 (56%) atypical Spitz tumors, and in 13 of 33 (39%) spitzoid melanomas (Table 1). We confirmed the expression of the chimeric ROS1, NTRK1, ALK, and RET proteins using immunohistochemistry. Cases harboring translocations showed moderate to strong staining for the corresponding fusion kinase, which was not observed in the cases lacking gene rearrangements. Patients with translocation-positive spitzoid

neoplasms were younger (median 21 years) than patients whose tumors did not harbor translocations (median 32.5 years; Mann Whitney test P<0.001).

ROS1 Fusions

ROS1 rearrangements were found in 19 of 73 (26%) Spitz nevi, 3 of 34 (8%) atypical Spitz tumors, and 3 of 33 (9%) spitzoid melanoma (Fig. 2a). The *ROS1* rearrangements fused the intact tyrosine kinase coding sequence of *ROS1* to the 5' portion of nine different partners (Fig. 1a and Supplementary Fig. S1-9). The expression of the chimeric ROS1 protein by immunohistochemistry was observed exclusively in cases with *ROS1* rearrangements (Fig. 2b and 2c). Expression of the *PWWP2A-ROS1* fusion construct in melan-a cells showed increased phosphorylation of the fusion protein, suggesting that the chimeric protein is constitutively active. Consistent with this, the MAPK and PI3K pathways were strongly activated compared to the GFP and the wild-type, full-length ROS1 controls. The phosphorylation of PWWP2A-ROS1, AKT, S6 and SHP2, but not ERK, was at least partially inhibited by crizotinib, an FDA-approved drug for lung cancer with *ALK* translocations that acts as an ALK[9] and ROS1[12] inhibitor (Fig. 2d).

ALK Fusions

We found *ALK* fusions in 8 of 75 (10.7%) Spitz nevi, 5 of 32 (15.6%) atypical Spitz tumors, and 1 of 33 (3%) spitzoid melanoma (Fig. 3a). Expression of the chimeric ALK protein was confirmed by immunohistochemistry and the rearrangements were validated in all cases with *ALK* fusions with FISH (Fig. 3b and 3c). Cases without *ALK* rearrangements by sequencing did not show ALK expression in immunohistochemistry or separated signals by FISH. *TPM3* and *DCTN1* were 5' fusion partners for *ALK* rearrangements (Fig. 1b and Supplementary Fig. S10-11). *TPM3-ALK* fusions were detected in 8 spitzoid neoplasms. *DCTN1* represents a novel fusion partner of *ALK*, was found in 6 cases, and resulted from a balanced translocation between homologous copies of chromosome 2 (Fig. 3d). Expression of the *DCTN1-ALK* fusion construct in melan-a cells showed increased phosphorylation of the fusion protein compared to the wild-type, full-length *ALK*, suggesting that the chimeric protein is constitutively active. Similar to the ROS1 fusions, AKT, ERK, and S6 were more phosphorylated in melan-a cells with the ALK fusion construct compared to the GFP control. Crizotinib inhibited the ALK fusion-induced activation of the oncogenic PI3K and MAPK signaling pathways (Fig. 3e).

NTRK1 Fusions

NTRK1 rearrangements were detected in 8 of 75 (10.7%) Spitz nevi, 8 of 32 (25%) atypical Spitz tumors, and 7 of 33 (21.2%) spitzoid melanoma (Fig. 4a). The expression of NTRK1 was confirmed with immunohistochemistry in cases with *NTRK1* fusions (Fig. 4b), but was absent in cases without *NTRK1* rearrangements. The *LMNANTRK1* fusions involved the novel fusion partner *LMNA* (localized at 1q22), and were caused by a 743 kb deletion of chromosome 1q, joining the first two exons of *LMNA* with *NTRK1* starting at exon 11 (Fig. 4c). The interchromosomal *TP53-NTRK1* translocation resulted from a fusion joining *NTRK1* starting from exon 9, containing the tyrosine kinase domain, to the 3'UTR of *TP53* (Fig. 1B and Supplementary Fig. S12-13). The expression of the *LMNA-NTRK1* fusion

construct in melan-a cells showed increased levels of phosphorylation of the fusion protein, AKT, ERK, S6 and PLCγ1 compared to the control cells. The strong activation of MAPK, PLCγ1 and PI3K pathways was inhibited by the NTRK1 inhibitor AZ-23 (Fig. 4d).

RET Fusions

We found *RET* fusions in 2 of 75 (2.7%) Spitz nevi, 1 of 32 (3.1%) atypical Spitz tumors, and 1 of 33 (3%) spitzoid melanoma (Fig. 5a). Fusions of *RET* on chromosome 10q11 involved the 5' fusion partners *KIF5B* on chromosome 10p11 and *GOLGA5* on chromosome 14q32 (Fig. 1b and Supplementary Fig. S14-15). In both fusions, the *RET* tyrosine kinase domain was fused to the coiled-coil domains of *KIF5B* (exons 1–16) or *GOLGA5* (exons 1-7). Immunohistochemical expression of RET was observed only in cases with *RET* translocations (Fig. 5b). Expression of the *GOLGA5-RET* fusion construct in melan-a cells showed increased phosphorylation of the fusion protein, AKT, ERK, S6, and PLCγ-1 compared to control cells. The phosphorylation of these proteins could be suppressed by vandetanib (Fig. 5c) or cabozantinib (Fig. 5d), which are both small molecule RET inhibitors that are FDA approved for medullary thyroid cancer.

BRAF Fusions

We identified gene rearrangements of the serine/threonine kinase *BRAF* in 4 of 75 (5.3%) Spitz nevi, 2 of 32 (6.3%) atypical Spitz tumors, and 1 of 33 (3%) spitzoid melanoma. The fusion genes contained *CEP89* exons 1–16 followed by the kinase domain of *BRAF* encoded by exons 9–18, or *LSM14A* exons 1-9 followed by *BRAF* exons 9-18, both resulting in loss of the auto-inhibitory, N-terminal RAS-binding domain of *BRAF* (Fig. 1b and Supplementary Fig. S16-17). In addition to the identified translocations, 1 of 75 (1.3%) Spitz nevi and 1 of 32 (3.1%) atypical Spitz tumors showed *BRAF* amplification as determined by at least 8 *BRAF* fusion signals per nucleus in interphase FISH.

Functional validation in xenograft models

To validate the oncogenic roles of the novel fusion kinases, we stably transduced mouse melan-a cells with *PWWP2A-ROS1, DCTN1-ALK, LMNA-NTRK1, GOLGA5-RET* fusions. We then injected the transduced cells subcutaneously and bilaterally into the flank of immunocompromised mice. We monitored the mice for the tumor formation every 3 to 4 days. Within 40 days, all injection sites in the fusion kinase groups (*PWWP2A-ROS1, DCTN1-ALK, LMNA-NTRK1, GOLGA5-RET*) developed rapidly growing tumors similarly to the one observed at the injection sites of melanocytes expressing the known melanoma oncogenes $HRAS^{G12V}$ and $NRAS^{G12V}$ (Supplementary Fig. S18). We observed no tumors at the injection sites in the control group with melanocytes that had been transduced with GFP.

DISCUSSION

Our results show that kinase fusions are important mechanisms of oncogene activation in spitzoid neoplasms. In aggregate, 72 of 140 (51.4%) spitzoid neoplasms harbored fusions involving the receptor tyrosine kinases *ROS1* (17%), *NTRK1* (16%), *ALK* (10%), *RET* (3%), and the serine/threonine kinase *BRAF* (5%). All fusions occurred in a mutually exclusive pattern (Fig. 1a), and no fusions were detected in tumors with *HRAS* mutations. All of the

sequenced kinase fusions created chimeric proteins that retained the intact kinase domain at the 3' end of the fusion transcript (Fig. 1b), a pattern similar to that observed in other cancers that harbor rearrangements involving these kinases.[13-15] All recombination sites between kinases and translocation partners involved the canonical intronic recombination sites, similar to those described in other types of cancers (*ROS1*: intron 33-35; *ALK*: intron 19; *NTRK1*: intron 8-10; *RET*: intron 11; *BRAF*: intron 8).[16] The majority of the novel 5' fusion partners identified in our study, namely those of *ROS1* (*PWWP2A*, *PPFIBP1*, *ERC1*, *MYO5A*, *CLIP1*, *HLA-A*, *KIAA1598* and *ZCCHC8*), *ALK* (*DCTN1*), *NTRK1* (*LMNA*), and *BRAF* (*CEP89* and *LSM14A*) contributed coiled-coil domains to the fusion proteins. The coiled-coil domains may play similar roles to the established 5' fusion partners (*TPM3*[17], *GOLGA5*[18], *KIF1B*[13]) of these kinases in promoting dimerization[19] and auto-activation of the kinases.[20]

Rearrangements of the kinases *ROS1*, *ALK*, *NTRK1*, *RET* and *BRAF* with similar fusion sites have previously been described in various types of aggressive tumors. *ROS1* fusions have been described in various cancer types, including lung carcinoma[21], glioblastoma[22], and cholangiocarcinoma.[23] *ALK* fusions have been described in anaplastic large cell lymphoma[17], lung cancer[14], inflammatory myofibroblastic tumors[24] and anecdotal studies have also reported *ALK* fusions in acral melanoma.[25] *RET* fusions, including the pericentric inversions giving rise to the *KIF5B-RET* fusion observed in spitzoid neoplasms, have been shown to drive lung cancer formation[13,15,26] and an interchromosomal *GOLGA5-RET* rearrangement was first described in papillary thyroid carcinomas occuring in children exposed to radioactive fallout from the Chernobyl nuclear accident.[18] *BRAF* fusions have been identified in pilocytic astrocytomas[27], papillary thyroid carcinoma[28], and rarely in melanocytic tumors.[29,30] In addition, our data that patients with translocation-positive spitzoid neoplasms were younger than patients whose tumors lacked translocations is similar to observations that lung cancers[15], thyroid cancers[18], and astrocytomas[27] harboring kinase fusions are more common in younger patients.

Our findings of the activated effector pathways downstream of the fusion kinases are in line with other experimental systems of cancer. For example, ubiquitous expression of constitutively active *RFP-RET* fusions in mice results in generalized melanocyte proliferation, formation of nevi and ultimately melanomas with MAPK pathway activation; this is similar to our finding of *GOLGA5-RET* fusions in spitzoid neoplasms.[31] Autocrine neurotrophin signaling involving *NTRK1* has been shown to promote proliferation and migration in melanoma cell lines[32], and constitutively active *NTRK1* activates MAPK and PI3K pathways in NIH-3T3 cells.[33] Phosphorylation of the MAPK and PI3K pathways is an essential component of oncogenic *ALK* signaling in lymphoma[17] and lung cancer[14], and we found that the novel fusion *DCTN1-ALK* has similar effects. The activation of the MAPK and PI3K pathways by the novel *PWWP2A-ROS1* fusion is also similar to the changes associated with other oncogenic *ROS1* fusions in various cancer types.[12,34] The results of our functional validation experiments in xenograft models are consistent with previous studies which showed that *TPM3-ROS1*[15], *EML4-ALK*[14], *KIF5B-RET*[13,15,26] fusions drive tumor formation in non-small cell lung cancers.

The common occurrence of kinase fusions in the entire biologic spectrum of spitzoid neoplasms (benign Spitz nevi, atypical Spitz tumors, spitzoid melanomas) suggests that these fusions occur early in the pathogenesis of spitzoid neoplasms. Therefore, kinase fusions are necessary, but not sufficient for malignant transformation, a situation analogous to that of mutations in oncogenes (such as *BRAF*, *NRAS*, *GNAQ* and *GNA11*) commonly found in melanocytic neoplasms. Consequently, the frequent kinase fusions described herein are unlikely to be useful in distinguishing benign from malignant spitzoid neoplasms.

Although the majority of spitzoid neoplasms behave in an indolent fashion, some spitzoid neoplasms metastasize and require systemic therapy. Lung cancers, lymphomas, and sarcomas with *ALK* or *ROS1* fusions, and thyroid cancers with *RET* fusions can be successfully treated using US Food and Drug Administration (FDA)-approved kinase inhibitors such as crizotinib, cabozantinib, and vandetanib. The fusion kinases identified here are therefore potential therapeutic targets for translocation-positive melanocytic tumors that require systemic therapy.

METHODS

Patients

The study was conducted according to the Declaration of Helsinki and human tissues were obtained with patient-informed consent under approval by the Institutional Review Boards/ Ethics Committees of Memorial Sloan-Kettering Cancer Center, New York, the University of California, San Francisco, and the Medical University of Graz, Austria. The excised skin lesions were fixed in 4% neutral buffered formalin, embedded in paraffin, processed using routine histologic methods and stained with hematoxylineosin. Specimens were collected over a time period of 6 months and the histopathologic diagnosis of Spitz nevus, atypical Spitz tumor, and spitzoid melanoma was confirmed by at least three dermatopathologists. Specimens with insufficient tissue amount or severely degraded nucleic acids were excluded. In total, specimens from 140 patients were analyzed and the clinical, histologic, and genetic characteristics are summarized in Supplementary Tables S1 and S2.

Targeted DNA sequencing

We sequenced 3230 exons from 182 cancer-related genes (Supplementary Table S3) and 37 introns of 14 genes (Supplementary Table S4) commonly rearranged genes in cancer with average depth-of-coverage of greater than 500x. Prior to DNA extraction, FFPE samples from all cases were reviewed to confirm that the tissue was of sufficient size to generate a minimum of 50ng of DNA and that this DNA would be derived from areas that contained a minimum of 20% melanocytic nuclei. DNA was isolated from 40μm thick sections of formalin-fixed, paraffin-embedded (FFPE) tissue. DNA sequencing was performed on indexed, adaptor ligation, hybridization-captured libraries (Agilent SureSelect custom kit). Sequencing was performed on the HiSeq-2000 instrument (Illumina), with 49x49 paired reads to an average depth of 997x (Supplementary Table S5).

RNA sequencing

Total RNA extracted from 40μm thick sections of FFPE tumor was reverse-transcribed with random hexamer primers using the SuperScript® III First-Strand Synthesis System (Invitrogen). Double stranded cDNA was synthesized with the NEBNext® mRNA Second Strand Synthesis Module (New England Biolabs).[35] Hybrid selection of indexed, adaptor-ligated libraries was performed using the cDNA Kinome hybridization kit with 612 transcripts of kinases and kinase-related genes (Agilent SureSelect Human Kinome Kit).[36] Selected libraries were sequenced on the HiSeq-2000 instrument (Illumina) with 49 x 49 paired reads. For RNA sequencing, we used a sequencing approach targeting 612 transcripts of kinases and kinase-related genes. We aimed for a high number of unique read pairs (≥ 50,000,000) per sample (Supplementary Table S6).

Sequence data analysis

Sequence data from gDNA and cDNA was mapped to the reference human genome (hg19) using the BWA aligner and processed using publically available SAMtools[37], Picard (http://picard.sourceforge.net) and GATK[38]. Genomic base substitutions and indels were detected using custom tools optimized for mutation calling in heterogeneous tumor samples, based on detecting common sequence variations and local sequence assembly. Variations were filtered using dbSNP and a custom artifact database, then annotated for known and likely somatic mutations using COSMIC. Copy number alterations were detected by comparing targeted genomic DNA sequence coverage with a process-matched normal control sample. Genomic rearrangements were detected by clustering chimeric reads mapping to targeted introns/exons. Expression levels were determined by analyzing cDNA sequence coverage of targeted exons.

Gene fusion confirmation

All gene fusions were validated by qRT-PCR from cDNA using the primers listed in Supplementary Table S7 and analysis on a Bioanalyzer (Agilent). Specific PCR amplicons were only detected with the appropriate combination of primers and template, and not with negative controls. The nucleotide sequence at the fusion site was confirmed by Sanger sequencing.

Interphase fluorescence in situ hybridization

A commercially available break-apart probe was used for *ALK* according to the manufacturer's protocol (Abbott, Des Plaines, IL). For *ROS1*, *RET*, *NTRK1*, and *BRAF*, break-apart fluorescence *in situ* hybridization (FISH) probes were prepared from BAC clones using standard procedures and labeled by nick translation with SpectrumGreen-dUTP and SpectrumRed-dUTP (Abbott, Des Plaines, IL). The following flanking BAC clones were used: *RET* (red: RP11-379D20, RP11-124O11; green: RP11-718J13, RP11-54P13), *NTRK1* (red: RP11-284F21, RP11-66D17; green: RP11-1038N13, RP11-1059C21), *ROS1* (red: RP11-379F24, RP11-103F10; green: RP11-1059G13, RP11-721K11), and *BRAF* (red: RP11-715H9, RP11-133N19; green: RP11-759K14, RP11-788O6). The probes were hybridized on 5μm-thick tissue sections, and the number and localization of the hybridization signals was assessed in a minimum of 100 interphase nuclei with well-

delineated contours and at least 50% of neoplastic cells had to show a split signal to report a rearrangement of a kinase.

Immunohistochemistry

Immunohistochemical analysis was performed on archival FFPE tumor specimens to confirm the expression of the fusion kinases and the activation of oncogenic pathways. We used a Discovery Ultra instrument with a multimer/DAB detection system (Ventana Medical Systems, Inc., Tucson, AZ) with appropriate negative and positive controls the following antibodies: ALK (clone D5F3; Cell Signaling, Danvers, MA; Dilution: 1:250), ROS1 (clone D4D6; Cell Signaling, Danvers, MA; Dilution: 1:25), NTRK1 (clone EP1058Y; Epitomics, Burlingame, CA; Dilution: 1:100), RET (clone EPR287; Epitomics, Burlingame, CA; Dilution: 1:250). The percentage of tumor cells exhibiting staining was scored by at least two independent pathologists.

Plasmids

To investigate the functional roles and the activation of oncogenic signaling pathways, we cloned *PWWP2A-ROS1*, *DCTN1-ALK*, *LMNA-NTRK1*, and *GOLGA5-RET* fusions and expressed them in melan-a cells (immortalized, non-tumorigenic mouse melanocytes). Expression vectors with green-fluorescent-protein (GFP) and the full- length, wild-type kinases *ROS1*, *ALK*, *NTRK1*, and *RET* were used as controls. Plasmids containing cDNAs of the genes of interest were obtained (Supplementary Table S8) and their sequences were verified.[39-41] Non-synonymous mutations deviating from the RefSeq sequence found in the *NTRK1* and *RET* plasmids were corrected using QuikChange site-directed mutagenesis (Agilent Technologies). Fusion constructs were generated by overlap extension.[42] Once PCR products containing the target cDNAs were generated, they were cloned into a pENTR vector using the pENTR/D-TOPO cloning kit (Life Technologies). All constructs were subsequently cloned into the pLenti6.3/TO/V5-Dest backbone (Life Technologies) and checked by digestion and sequencing. The larger fusion genes involving *ALK* and *ROS1* were also cloned into the PBX2.1 backbone of the PiggyBac Transposon system.[43]

Stably transduced Melan-a cells

Melan-a cells were generously provided by Dr. Dorothy C Bennett (St. George's Hospital, University of London, London, UK)[44] and maintained in glutamine-containing RPMI-1640 supplemented with 10% heat-inactivated fetal bovine serum, 200 nM of 12-O-tetradecanoylphorbol-13-acetate (TPA), penicillin (100 units/mL) and streptomycin (50 mg/mL). 293FT cells were purchased from Life Technologies and maintained in DME-H21 medium containing 10% heat inactivated fetal bovine serum, MEM Non-Essential Amino Acids (0.1 mM), sodium pyruvate (1 mM), penicillin (100 units/mL) and streptomycin (50 mg/mL).

Lentiviruses were produced by transfecting 293FT cells with plasmid DNA in a pLenti6.3/TO/V5-Dest backbone together with ViraPowerTM (Life Technologies) according to the manufacturer's protocol. Infections of melan-a cells were conducted in the presence of 10μg/ml of Polybrene (Santa Cruz Biotechnology). Stably transduced melan-a cells expressing *GOLGA5-RET*, *LMNA-NTRK1*, *PWWP2A-ROS1*, *RET*, and *NTRK1* were

generated by infection with the respective lentivirus. *ALK* and *ROS1* expressing melan-a cell lines were generated by cotransfection of the PBX2.1 construct together with pCMV-HyPBase transposase vector. Melan-a cell lines stably expressing GFP were generated using pLenti6.2/V5 and PBX2.1 vectors and used as a control. Cells were selected for at least 20 days using 5 μg/ml of blasticidin S-hydrochloride (Life Technologies) after transduction.

Western Blotting

Anti-RET (#3220), anti-phospho-RET (Tyr905) (#3221), anti-ALK (#3791), anti-phospho-ALK (Tyr1096) (#6962), anti-ROS1 (#3266), anti-phospho ROS1 (Tyr2274) (#3078), anti-phospho-p44/42 MAPK (Erk1/2) (Thr202/Tyr204) (#9101), anti-AKT (#9272), anti-phospho-AKT (Ser473) (#9271), anti-S6 Ribosomal Protein (#2317), anti-phospho-S6 Ribosomal Protein (Ser235/236) (#2211), anti-p-PLCγ1 (#2822), anti-phospho-PLCγ1 (Tyr783) (#2821), anti-SHP2 (D50F2) (#3397), anti-phospho-SHP2 (Tyr 542) (#3751), as well as the secondary antibodies anti-rabbit IgG-HRP (#7076) and anti-mouse IgG-HRP (#7074) were purchased from Cell Signaling Technology (Danvers, MA). Anti-HSP60 (sc-1722) and anti-ERK2 (C-14) (sc- 154) as well as the secondary antibodies anti-goat IgG-HRP (sc-2033) were purchased from Santa Cruz Biotechnology (Santa Cruz, CA). Anti-TrkA (ab37837) and anti-phospho-TrkA (Tyr408) (ab1445) were purchased from Abcam (Cambridge, MA).

Cell lysates were prepared in RIPA buffer supplemented with Halt protease and phosphatase inhibitor cocktail (Thermo Scientific). Equal amounts of protein, as measured by BCA protein assay, were resolved in 4-12% Bis-Tris NuPage gradient gels (Life Technologies) and transferred electrophoretically onto a PVDF 0.45-micron membrane. Membranes were blocked for 1 hour at room temperature in 5% BSA or non-fat milk in TBST before being incubated overnight at 4°C with the primary antibodies. All primary antibodies were diluted 1:1000 in 5% BSA or non-fat milk in TBST. After 3 washes of 5 minutes in TBST, secondary antibodies were diluted 1:3000 in 5% non-fat milk in TBST and incubated for 1 hour at room temperature. After another 3 washes in TBST, detection of the signal was achieved by incubating the membrane on an ECL solution from Millipore and exposure on autoradiography films from Denville Scientific (Metuchen, NJ).

Drug studies

Vandetanib and cabozantinib were purchased from Selleckchem (Houston, TX). Crizotinib was purchased from Chemie Tek (Indianapolis, IN). AZ-23 was purchased from Axon Medchem (Groningen, The Netherlands).

Tumorigenicity study

Animal experiments were carried out in accordance with the Declaration of Helsinki and were approved by the ethical committee of the University of California, San Francisco. 1.5 million melan-a cells stably transduced with the indicated oncogene or GFP control vector were injected subcutaneously in two separate, 6 week old female NOD-scid, IL2-Rγ^{null} mice. Mice were palpated 3 times a week for the development of tumors over a period of 40 days.

Supplementary Material

Refer to Web version on PubMed Central for supplementary material.

Acknowledgments

This work was funded by grants from the National Institutes of Health R01 CA131524 and P01 CA025874 (to B.C.B.) and P30 CA008748 (to MSKCC), the American Skin Association (to B.C.B.), the Jubilaeumsfonds of the Oesterreichische Nationalbank OeNB (to L.C. and T.W.), the Harry J. Lloyd Trust - Translational Research Grant (to T.W.), and a Charles H. Revson Senior Fellowship (to T.W.). We thank Dr. Margaret Leversha and Kalyani Chadalavada for assisting with FISH, and Dr. Achim Jungbluth for assisting with IHC.

REFERENCES

1. Spitz S. Melanomas of childhood. Am J Pathol. 1948; 24:591–609. [PubMed: 18859360]
2. Ludgate MW, et al. The atypical Spitz tumor of uncertain biologic potential: a series of 67 patients from a single institution. Cancer. 2009; 115:631–41. [PubMed: 19123453]
3. Murali R, et al. Sentinel lymph node biopsy in histologically ambiguous melanocytic tumors with spitzoid features (so-called atypical spitzoid tumors). Ann Surg Oncol. 2008; 15:302–9. [PubMed: 18000712]
4. Flaherty KT, Hodi FS, Fisher DE. From genes to drugs: targeted strategies for melanoma. Nature reviews. Cancer. 2012; 12:349–61. [PubMed: 22475929]
5. Bastian BC, LeBoit PE, Pinkel D. Mutations and copy number increase of HRAS in Spitz nevi with distinctive histopathological features. Am J Pathol. 2000; 157:967–72. [PubMed: 10980135]
6. Wiesner T, et al. Germline mutations in BAP1 predispose to melanocytic tumors. Nat Genet. 2011; 43:1018–21. [PubMed: 21874003]
7. Wiesner T, et al. A distinct subset of atypical Spitz tumors is characterized by BRAF mutation and loss of BAP1 expression. Am J Surg Pathol. 2012; 36:818–30. [PubMed: 22367297]
8. Chapman PB, et al. Improved survival with vemurafenib in melanoma with BRAF V600E mutation. N Engl J Med. 2011; 364:2507–16. [PubMed: 21639808]
9. Kwak EL, et al. Anaplastic lymphoma kinase inhibition in non-small-cell lung cancer. N Engl J Med. 2010; 363:1693–703. [PubMed: 20979469]
10. Druker BJ, et al. Efficacy and safety of a specific inhibitor of the BCR-ABL tyrosine kinase in chronic myeloid leukemia. N Engl J Med. 2001; 344:1031–7. [PubMed: 11287972]
11. Vogelstein B, et al. Cancer genome landscapes. Science. 2013; 339:1546–58. [PubMed: 23539594]
12. Bergethon K, et al. ROS1 rearrangements define a unique molecular class of lung cancers. J Clin Oncol. 2012; 30:863–70. [PubMed: 22215748]
13. Lipson D, et al. Identification of new ALK and RET gene fusions from colorectal and lung cancer biopsies. Nat Med. 2012; 18:382–4. [PubMed: 22327622]
14. Soda M, et al. Identification of the transforming EML4-ALK fusion gene in non-small-cell lung cancer. Nature. 2007; 448:561–6. [PubMed: 17625570]
15. Takeuchi K, et al. RET, ROS1 and ALK fusions in lung cancer. Nat Med. 2012; 18:378–81. [PubMed: 22327623]
16. Forbes SA, et al. COSMIC: mining complete cancer genomes in the Catalogue of Somatic Mutations in Cancer. Nucleic Acids Res. 2011; 39:D945–50. [PubMed: 20952405]
17. Lamant L, Dastugue N, Pulford K, Delsol G, Mariame B. A new fusion gene TPM3-ALK in anaplastic large cell lymphoma created by a (1;2)(q25;p23) translocation. Blood. 1999; 93:3088–95. [PubMed: 10216106]
18. Rabes HM, et al. Pattern of radiation-induced RET and NTRK1 rearrangements in 191 post-chernobyl papillary thyroid carcinomas: biological, phenotypic, and clinical implications. Clin Cancer Res. 2000; 6:1093–103. [PubMed: 10741739]
19. Cohen C, Parry DA. Alpha-helical coiled coils: more facts and better predictions. Science. 1994; 263:488–9. [PubMed: 8290957]

20. McWhirter JR, Galasso DL, Wang JY. A coiled-coil oligomerization domain of Bcr is essential for the transforming function of Bcr-Abl oncoproteins. Mol Cell Biol. 1993; 13:7587–95. [PubMed: 8246975]
21. Rikova K, et al. Global survey of phosphotyrosine signaling identifies oncogenic kinases in lung cancer. Cell. 2007; 131:1190–203. [PubMed: 18083107]
22. Birchmeier C, Sharma S, Wigler M. Expression and rearrangement of the ROS1 gene in human glioblastoma cells. Proc Natl Acad Sci U S A. 1987; 84:9270–4. [PubMed: 2827175]
23. Gu TL, et al. Survey of tyrosine kinase signaling reveals ROS kinase fusions in human cholangiocarcinoma. PLoS One. 2011; 6:e15640. [PubMed: 21253578]
24. Lawrence B, et al. TPM3-ALK and TPM4-ALK oncogenes in inflammatory myofibroblastic tumors. Am J Pathol. 2000; 157:377–84. [PubMed: 10934142]
25. Niu HT, et al. Identification of anaplastic lymphoma kinase break points and oncogenic mutation profiles in acral/mucosal melanomas. Pigment Cell Melanoma Res. 2013
26. Kohno T, et al. KIF5B-RET fusions in lung adenocarcinoma. Nat Med. 2012; 18:375–7. [PubMed: 22327624]
27. Jones DT, et al. Tandem duplication producing a novel oncogenic BRAF fusion gene defines the majority of pilocytic astrocytomas. Cancer Res. 2008; 68:8673–7. [PubMed: 18974108]
28. Ciampi R, et al. Oncogenic AKAP9-BRAF fusion is a novel mechanism of MAPK pathway activation in thyroid cancer. J Clin Invest. 2005; 115:94–101. [PubMed: 15630448]
29. Palanisamy N, et al. Rearrangements of the RAF kinase pathway in prostate cancer, gastric cancer and melanoma. Nat Med. 2010; 16:793–8. [PubMed: 20526349]
30. Botton T, et al. Recurrent BRAF kinase fusions in melanocytic tumors offer an opportunity for targeted therapy. Pigment Cell Melanoma Res. 2013
31. Kato M, et al. Transgenic mouse model for skin malignant melanoma. Oncogene. 1998; 17:1885–8. [PubMed: 9778055]
32. Truzzi F, et al. Neurotrophins and their receptors stimulate melanoma cell proliferation and migration. J Invest Dermatol. 2008; 128:2031–40. [PubMed: 18305571]
33. Reuther GW, Lambert QT, Caligiuri MA, Der CJ. Identification and characterization of an activating TrkA deletion mutation in acute myeloid leukemia. Mol Cell Biol. 2000; 20:8655–66. [PubMed: 11073967]
34. Jun HJ, et al. The oncogenic lung cancer fusion kinase CD74-ROS activates a novel invasiveness pathway through E-Syt1 phosphorylation. Cancer Res. 2012; 72:3764–74. [PubMed: 22659450]
35. D'Alessio JM, Gerard GF. Second-strand cDNA synthesis with E. coli DNA polymerase I and RNase H: the fate of information at the mRNA 5′ terminus and the effect of E. coli DNA ligase. Nucleic Acids Res. 1988; 16:1999–2014. [PubMed: 2833725]
36. Levin JZ, et al. Targeted next-generation sequencing of a cancer transcriptome enhances detection of sequence variants and novel fusion transcripts. Genome Biol. 2009; 10:R115. [PubMed: 19835606]
37. Li H, et al. The Sequence Alignment/Map format and SAMtools. Bioinformatics. 2009; 25:2078–9. [PubMed: 19505943]
38. McKenna A, et al. The Genome Analysis Toolkit: a MapReduce framework for analyzing next-generation DNA sequencing data. Genome Res. 2010; 20:1297–303. [PubMed: 20644199]
39. Scaffidi P, Misteli T. Lamin A-dependent misregulation of adult stem cells associated with accelerated ageing. Nat Cell Biol. 2008; 10:452–9. [PubMed: 18311132]
40. Johannessen CM, et al. COT drives resistance to RAF inhibition through MAP kinase pathway reactivation. Nature. 2010; 468:968–72. [PubMed: 21107320]
41. Yano H, Cong F, Birge RB, Goff SP, Chao MV. Association of the Abl tyrosine kinase with the Trk nerve growth factor receptor. J Neurosci Res. 2000; 59:356–64. [PubMed: 10679771]
42. Heckman KL, Pease LR. Gene splicing and mutagenesis by PCR-driven overlap extension. Nat Protoc. 2007; 2:924–32. [PubMed: 17446874]
43. Choi HJ, et al. ECM-dependent HIF induction directs trophoblast stem cell fate via LIMK1-mediated cytoskeletal rearrangement. PLoS One. 2013; 8:e56949. [PubMed: 23437279]

44. Bennett DC, Cooper PJ, Hart IR. A line of non-tumorigenic mouse melanocytes, syngeneic with the B16 melanoma and requiring a tumour promoter for growth. Int J Cancer. 1987; 39:414–8. [PubMed: 3102392]

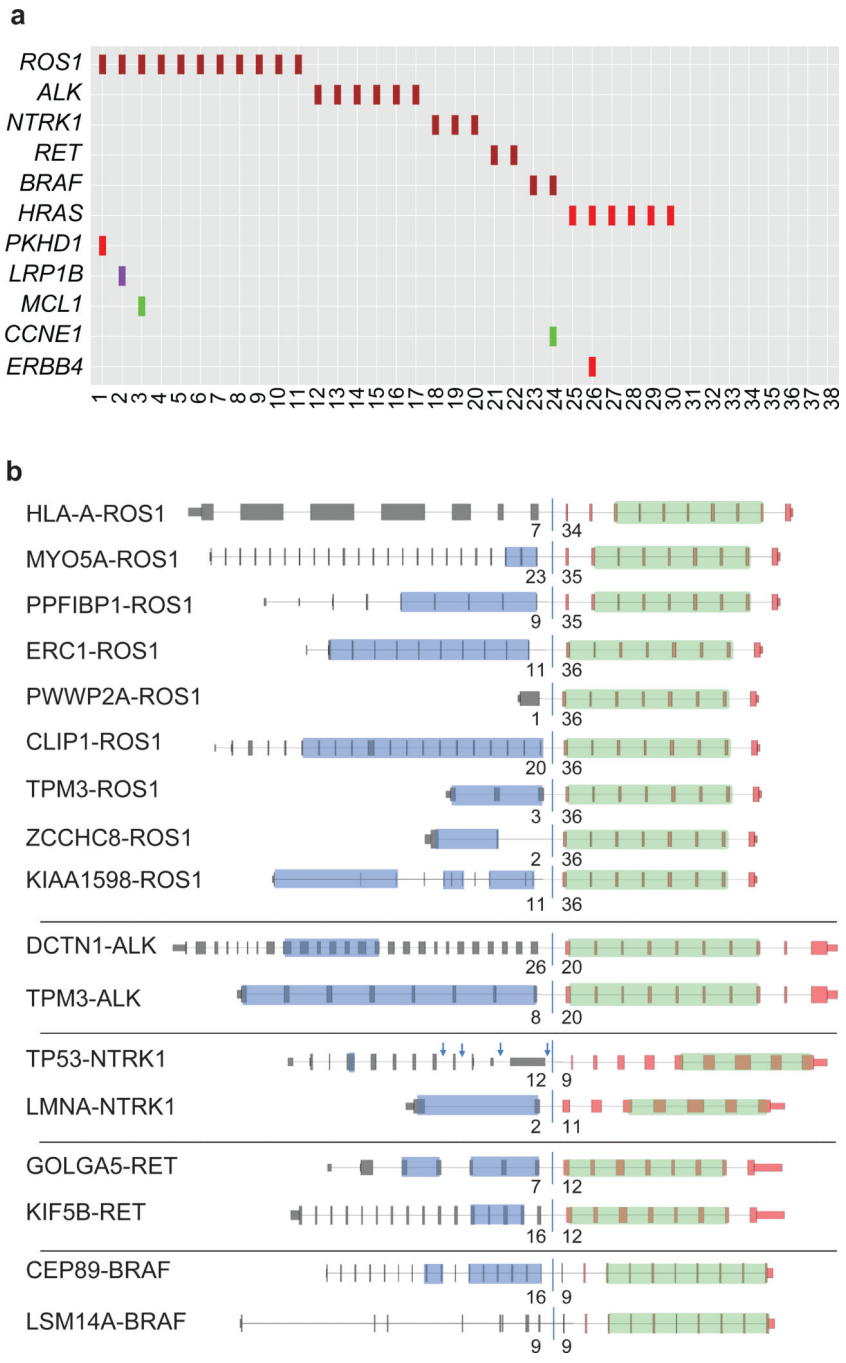

Figure 1. Genomic aberrations identified in 38 spitzoid neoplasms by targeted sequencing.

(**a**) The columns denote the samples, the rows denote genes, purple squares represent gene fusions, red squares symbolize point mutations and indels, green squares denote gene amplifications, and purple squares indicate truncating mutations. The identified fusion genes and *HRAS* mutations were mutually exclusive in 38 spitzoid neoplasms. Mutations in *PKHD1*, *ERBB4*, *LRP1B*, and amplifications of *MCL1* and *CCNE1* are of unknown significance and co-occurred with kinase fusions and HRAS mutations. (**b**) Illustration of the distinct fusion genes for the *ROS1*, *ALK*, *NTRK1*, *RET*, and *BRAF* rearrangements. The

grey bars represent the exons of the genes, the numbers below the bars the exon number, and the blue line the predicted breakpoints. The green shaded areas indicate the kinase domain and the blue shaded areas the coiled-coil domain of the fusion gene product. In the *TP53-NTRK1* fusion transcript, multiple breakpoints spanning exon 8-12 of TP53 were predicted.

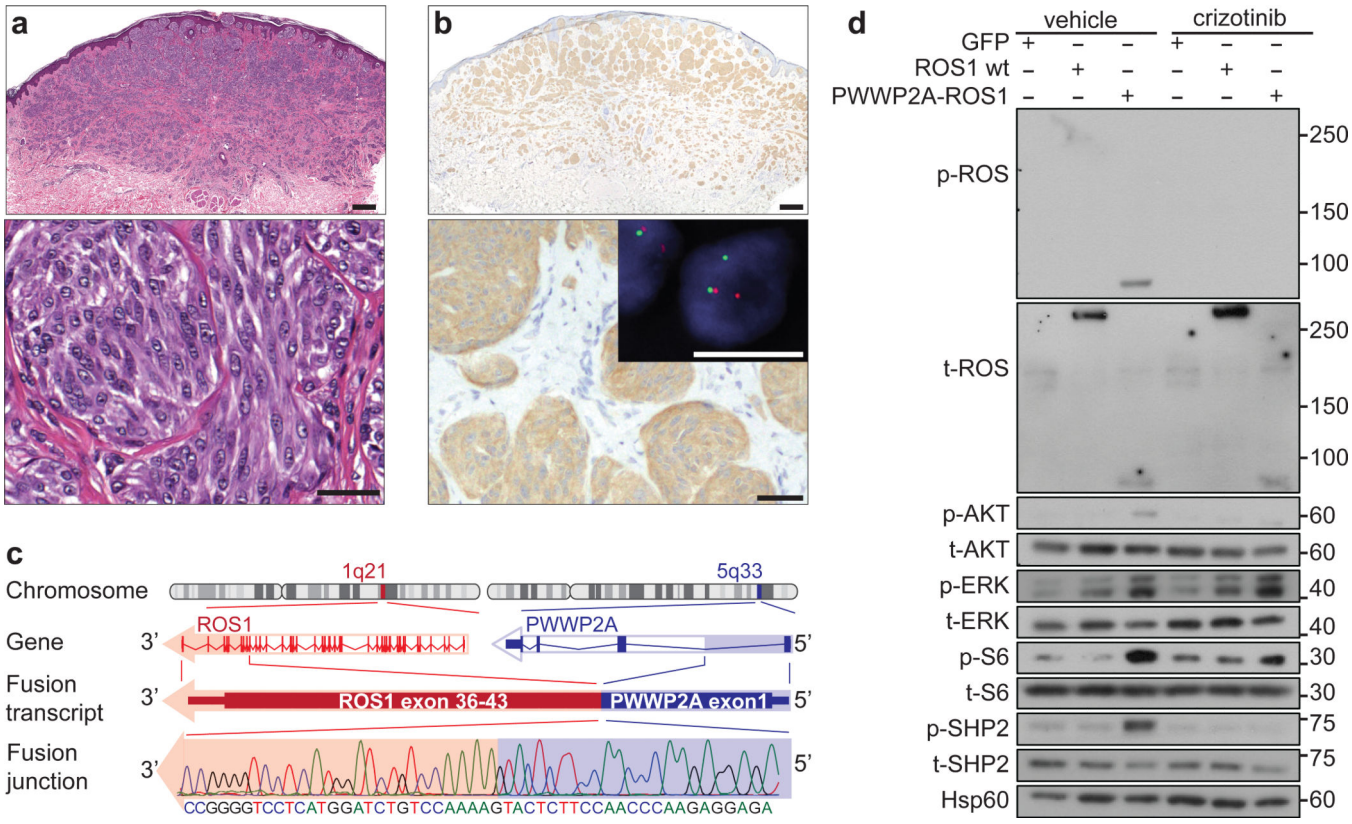

Figure 2. *ROS1* fusions

(**a**) Histologic section of an atypical Spitz tumor with *PWWP2A-ROS1* fusion from the gluteal region of a 55-year-old female (hematoxylin and eosin stain). Scale bar, 500μm. Scale bar magnification, 50μm. (**b**) Immunohistochemistry for ROS1 shows expression in the melanocytes; stromal cells serve as internal negative controls. Scale bar, 500μm. Scale bar magnification, 50μm. The FISH inset confirms the gene rearrangements using breakpoint flanking FISH probes. The rearranged *ROS1* locus appears as individual green and red signals, and the wild type kinase allele with juxtaposed green/red signals. Scale bar, 10μm. (**c**) Illustration of the *PWWP2A-ROS1* kinase fusion. *ROS1* is located on chromosome 1q21, and *PWWP2A* on chromosome 5q33. Due to genomic rearrangements, exon 1 of *PWWP2A* is fused with exon 36 to 43 of *ROS1*, which contains the tyrosine kinase domain. The in-frame fusion junction of the transcript was confirmed by Sanger sequencing. (**d**) The *PWWP2A-ROS1* fusion, but not the control-GFP construct, induces p-AKT, p-ERK, p-S6, and p-SHP2 in melan-a cells. Crizotinib inhibited at least partially the phosphorylation of the chimeric PWWP2A-ROS1 fusion protein, p-AKT, p-S6, and p-SHP2. The indicated protein weight markers in kDa are estimated from molecular weight standards. Results are representative of three independent experiments.

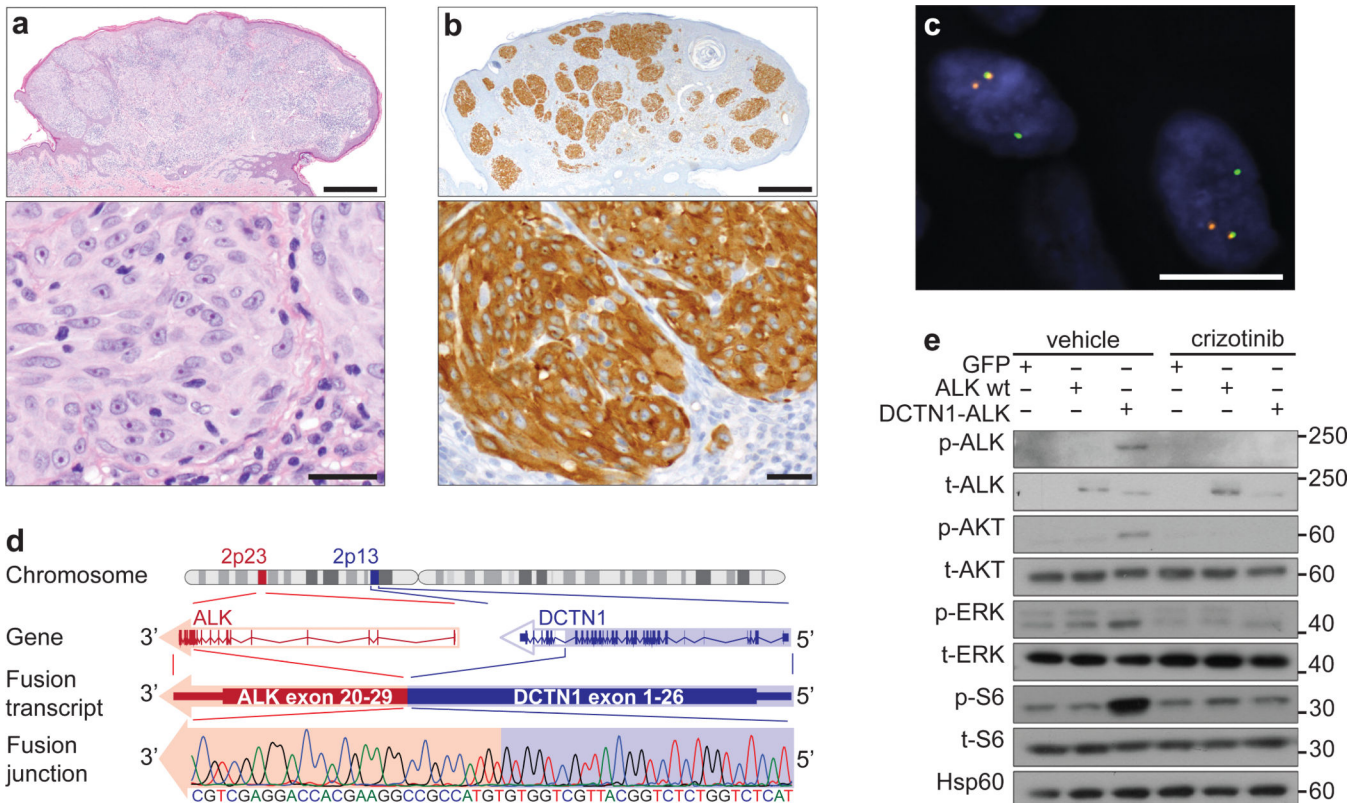

Figure 3. *ALK* fusions

(**a**) Histologic section of an atypical Spitz tumor excised from the upper arm of a 19-year-old male with a *DCTN1-ALK* fusion (hematoxylin and eosin stain). Scale bar, 500μm. Scale bar magnification, 50μm. (**b**) Immunohistochemistry shows ALK expression in the melanocytes; stromal cells serve as internal negative controls. Scale bar, 500μm. Scale bar magnification, 50μm. (**c**) FISH demonstrates the *ALK* gene rearrangement by the individual green and orange signals using breakpoint flanking probes. Scale bar, 10μm. (**d**) Illustration of the *DCTN1-ALK* kinase fusion. *ALK* is located on chromosome 1p23 and *DCTN1* on chromosome 2p13. Due to genomic rearrangements, exon 1-26 of *DCTN1* is fused with exon 20 to 29 of *ALK*, which contains the tyrosine kinase domain. The in-frame junction of the fusion transcript was confirmed with Sanger sequencing. (**e**) The *DCTN1-ALK* fusion construct, but not the control-GFP construct, induces p-AKT, p-ERK and p-S6 in melan-a cells. These effects and the phosphorylation of chimeric DCTN1-ALK protein can be inhibited with crizotinib. The indicated protein weight markers in kDa are estimated from molecular weight standards. Results are representative of three independent experiments.

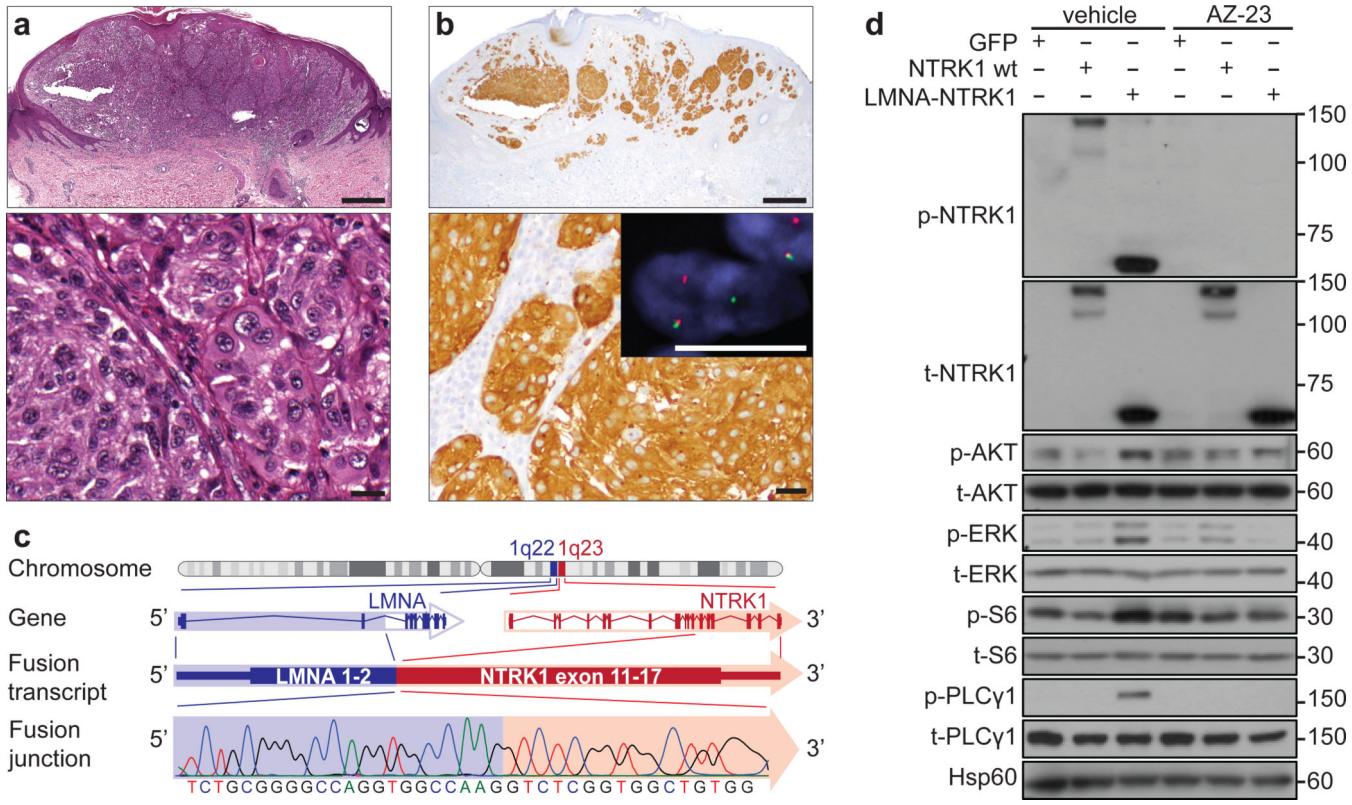

Figure 4. *NTRK1* fusions

(**a**) Histologic section of a spitzoid melanoma excised from the left knee of a 39-year-old woman with an *LMNA-NTRK1* fusion (hematoxylin and eosin stain). Scale bar, 500μm. Scale bar magnification, 50μm. (**b**) Immunohistochemistry demonstrates the NTRK1 expression in melanocytes; stromal cells serve as internal negative controls. Scale bar, 500μm. Scale bar magnification, 50μm. The FISH inset confirms the gene rearrangements using breakpoint flanking FISH probes by the individual green and red signals. Scale bar, 10μm. (**c**) The *LMNA-NTRK1* kinase fusion is caused by a 743kb deletion on chromosome 1q, joining the first 2 exons of *LMNA* with exon 11 to 17 of *NTRK1*. The in-frame junction of the fusion transcript was confirmed with Sanger sequencing. (**d**) The *LMNA-NTRK1* fusion construct, but not the full-length, wild-type NTRK1 or the control-GFP constructs induce p-AKT, p-ERK, pS6 and p-PLCγ1 in melan-a cells. A small molecule kinase inhibitor, AZ-23, inhibited the phosphorylation of LMNA-NTRK1 and the activation of the oncogenic signaling pathways. The indicated protein weight markers in kDa are estimated from molecular weight standards. Results are representative of three independent experiments.

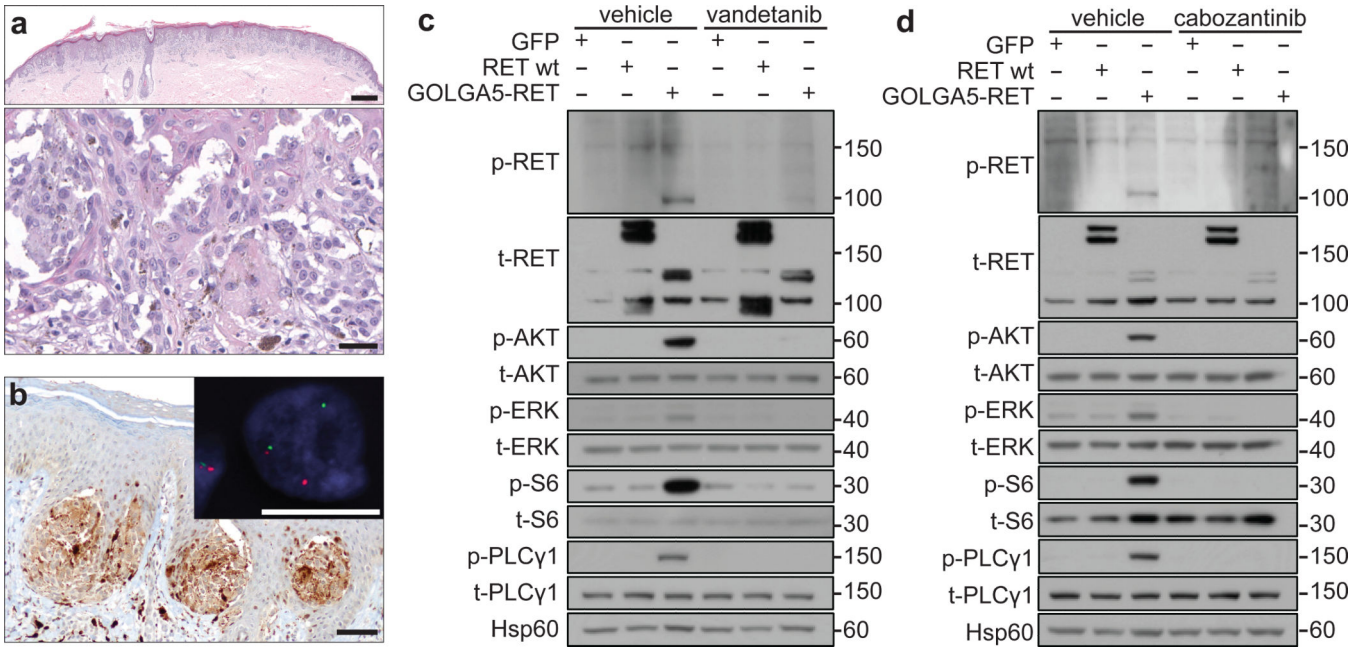

Figure 5. RET fusions

(**a**) Histologic section of a pigmented spindle cell nevus (a morphologic variant of Spitz nevus) from a 50-year-old woman with a *GOLGA5-RET* fusion (hematoxylin and eosin stain). Scale bar, 500μm. Scale bar magnification, 50μm. (**b**) RET expression in melanocytes; keratinocytes serve as internal negative controls. Scale bar, 100μm. The individual green and red signals in FISH confirm the gene rearrangements using breakpoint flanking FISH probes. Scale bar, 10μm. (**c, d**) The *GOLGA5-RET* construct, but not the wild-type, full-length RET or the control-GFP constructs, induces p-AKT, p-ERK, p-S6, and p-PLCγ1 in melan-a cells. The activation of these pathways and the phosphorylation of GOLGA5-RET can be inhibited with (**c**) vandetanib and (**d**) cabozantinib. The indicated protein weight markers in kDa are estimated from molecular weight standards. Results are representative of three independent experiments.

Table 1

Frequency of kinase fusions in spitzoid neoplasms.

Fusion	Spitz nevus (n=75) % (number of cases)	Atypical Spitz tumor (n=32) % (number of cases)	Spitzoid melanoma (n=33) % (number of cases)	Total (n=140) % (number of cases)
ROS1	**25.3%** (19)	**6.3%** (2)	**9.1%** (3)	**17.1%** (24)
ALK	**10.7%** (8)	**15.6%** (5)	**3%** (1)	**10%** (14)
NTRK1	**10.7%** (8)	**25%** (8)	**21.2%** (7)	**16.4%** (23)
BRAF	**5.3%** (4)	**6.3%** (2)	**3%** (1)	**5%** (7)
RET	**2.7%** (2)	**3.1%** (1)	**3%** (1)	**2.9%** (4)
Total	**54.7%** (41)	**56.3%** (18)	**39.4%** (13)	**51.4%** (72)